Nano Energy 49 (2018) 634–643

Contents lists available at ScienceDirect

Nano Energy

journal homepage: www.elsevier.com/locate/nanoen

Full paper

Controllable etching of MoS_2 basal planes for enhanced hydrogen evolution through the formation of active edge sites

Zegao Wang[a], Qiang Li[a,b], Haoxiang Xu[c], Christian Dahl-Petersen[a,d], Qian Yang[a], Daojian Cheng[c], Dapeng Cao[c], Flemming Besenbacher[a], Jeppe V. Lauritsen[a], Stig Helveg[d], Mingdong Dong[a,e,*]

[a] Interdisciplinary Nanoscience Center (iNANO), Aarhus University, DK-8000 Aarhus C, Denmark
[b] Key Laboratory for Colloid and Interface Chemistry, Ministry of Education, Shandong University, Jinan 250100, China
[c] State Key Laboratory of Organic-Inorganic Composites, Beijing University of Chemical Technology, Beijing 100029, China
[d] Haldor Topsoe A/S, Haldor Topsøes Allé 1, DK-2800 Kgs. Lyngby, Denmark
[e] Department of Chemistry, Stanford University, Stanford, CA 94305, United States

ARTICLE INFO

Keywords:
Molybdenum disulfide
Nanostructure
Steam vapor
Hydrogen evolution
Electrochemical microcell

ABSTRACT

The catalytic activity of molybdenum disulfide (MoS_2) is associated with active sites located along the edges, whereas the MoS_2 basal plane is regarded to be inert. However, it is a great challenge to develop a rational way for producing active edges efficiently. Herein, we report a novel, cost-effective top-down process in which we can create a high density of active edge sites on MoS_2 basal plane by selective steam etching. The results show that the etched structure is strongly sensitive to the temperature, which creates 1D nano-channels, 2D in-plane triangular pits and 3D vertical hexagonal cavities on the MoS_2 basal planes by elevating the temperature. The edge configuration is revealed to exhibit a distinct crystallographic orientation. Furthermore, we evaluate the corresponding enhanced electrocatalytic activity for the hydrogen evolution reaction (HER) by measurements of the single etched MoS_2 samples in an electrochemical microcell, where the Tafel slope decrease by 49%, confirming the increased the density of active sites. In addition, the method is not limited to 2D materials in a flat geometry alone, but is also demonstrated on 0D MoS_2 particles by *in-situ* transmission electron microscopy. The steam etching reported here offers an alternative avenue to engineer the surface structures of MoS_2 facilitating the electrocatalytic applications of MoS_2 for hydrogen production.

1. Introduction

Owing to its low cost and high catalytic activity, molybdenum disulfide (MoS_2) has shown great promise as an alternative earth-abundant catalyst to replace platinum in the hydrogen evolution reaction (HER) used in electrochemical generation of hydrogen from water [1–5]. Experimental and theoretical studies have demonstrated that the catalytic activity arises entirely from the active sites located along the edges of MoS_2, while the unperturbed basal planes of MoS_2 are catalytically inert [3–7]. Many elaborate materials design strategies aimed at increasing the density of active sites at the surface of pristine MoS_2 have been reported, such as defect and substrate engineering [8–12], phase-engineering and nanostructure formation [13–18]. So far, most of the current approaches focus on synthesizing nanostructured MoS_2 by the bottom-up method, however, the top-down method may provide an alternative and facile process with high yield.

Chemical etching is already an effective top-down method to engineer the surface structures of materials through creation of fresh edges and nanoscale pores [19–21]. Recently, it has been reported that MoS_2 thin films could be thinned and etched by directly using H_2, XeF_2 and CF_4 et al. [22–24]. However, the noxious reactants are involved; the formation of side-products and the complex etching process limits its practical applications. Herein, a simple and environmentally friendly steam treatment method has been developed with demonstrated ability to create various densities of MoS_2-edge sites within the inert basal planes of MoS_2 by controlling the temperature and vapor pressure of water. By this method, 1D nano-channels, 2D in-plane triangular pits and 3D vertical out-of-plane cavities are controllably etched on the planar surface of bulk MoS_2. Furthermore, the etching behavior is also demonstrated by time resolved *in-situ* TEM on curved, but still well-defined MoS_2 nanostructures resulting from technical catalyst preparation protocols. Finally, the catalytic activity is quantitatively evaluated by fabricating an electrochemical microcell based on individual steam etched MoS_2 flakes, which, by comparison with pristine MoS_2, demonstrated that the Tafel slope decrease by 49.7%. Finally, the simulation based on density functional theory confirms that the enhanced catalytic activity is not only due to the introduced edge sites, but also the edge-proximity MoS_2 basal plane, where the adsorption free energy of hydrogen atom on edge-closed MoS_2 basal plane is smaller than that of on pristine MoS_2 basal plane.

* Corresponding author at: Interdisciplinary Nanoscience Center (iNANO), Aarhus University, DK-8000 Aarhus C, Denmark.
E-mail address: dong@inano.au.dk (M. Dong).

https://doi.org/10.1016/j.nanoen.2018.04.067
Received 13 January 2018; Received in revised form 9 April 2018; Accepted 26 April 2018
Available online 05 May 2018

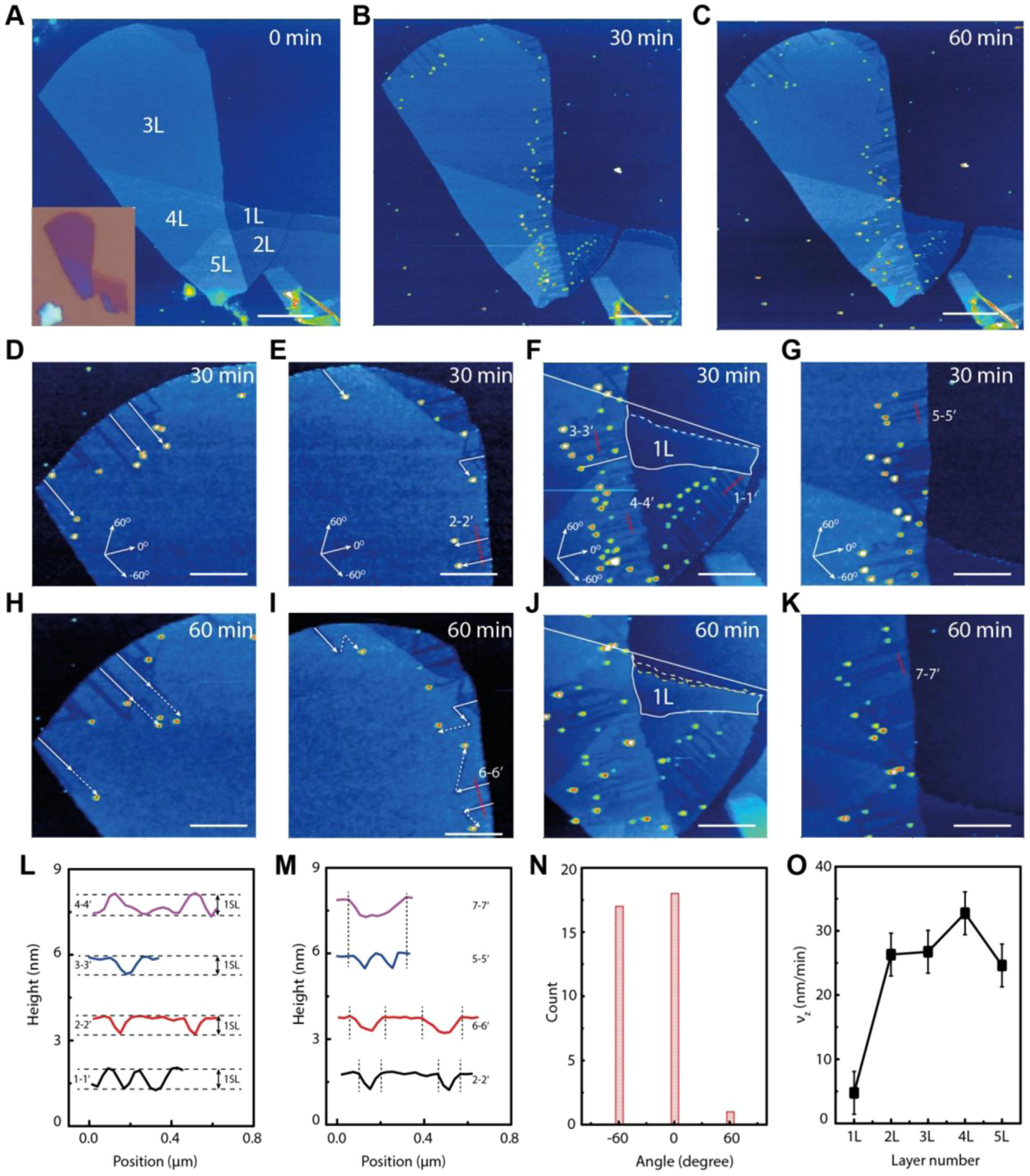

Fig. 1. 1D steam vapor etching of MoS_2. (**A**) The as-prepared 1–5 L MoS_2, the inset is the optical image. (**B**, **C**) The AFM images of 1–5 L MoS_2 after etching for 30 min and additional 30 min at 500 °C, respectively. (**D**-**G**) High-resolution AFM images from (B). (**H**-**K**) High-resolution AFM images from (C). The dash lines in (F) and (J) are the edges of monolayer MoS_2 edges before and after 30 min etching. (**L**) Line-profiles of the nano-channels corresponding to the red lines marked in (E) and (F). (**M**) Line-profiles of the nano-channels corresponding to the red lines marked in (E), (I), (G) and (H). (**N**) The distribution of the etching angle. (**O**) The etching speed on 1–5 L MoS_2. The scale bars in (A)-(C) are 2 μm, and in (D)-(K) are 1 μm. (For interpretation of the references to color in this figure legend, the reader is referred to the web version of this article.)

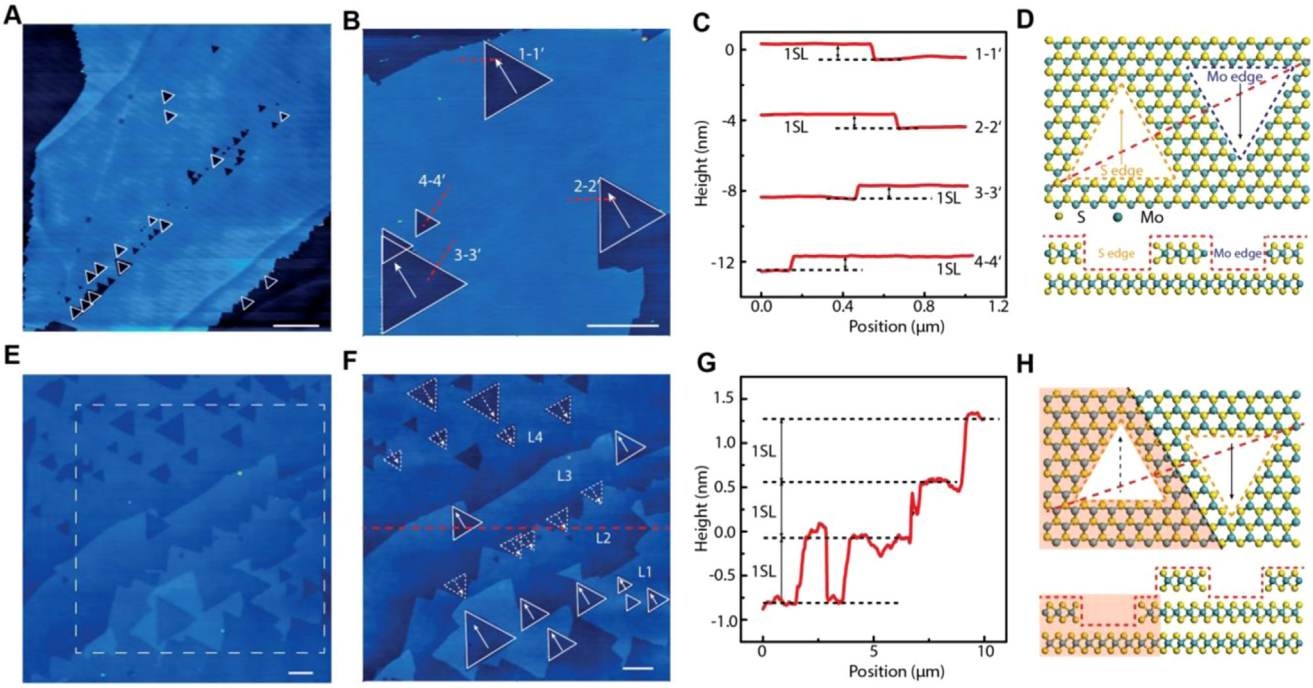

Fig. 2. 2D steam vapor etching of bulk MoS_2. (**A**) A typical AFM image of MoS_2 on SiO_2 after steam etching at 600 °C for 30 min (**B**) The high-resolution AFM image of the triangular pits. (**C**) Line-profiles corresponding to the dashed red lines marked in (B). (**D**) Schematic drawing of hexagonal lattice of the MoS_2 with one single layer depth triangular pits and the side-view along the dash line. (**E**) AFM image of the etched MoS_2 located on different layers. (**F**) zoom-in AFM image of the dashed white square in (E). (**G**) Line-profiles corresponding to the dashed red lines marked in (F). (**H**) Schematic drawing of two triangular pits on adjacent MoS_2 layers and the side-view along the dash line. The scale bars in (A), (B), (E) and (F) are 1 μm. (For interpretation of the references to color in this figure legend, the reader is referred to the web version of this article.)

2. Results and discussion

2.1. 1D steam vapor etching of MoS_2

The steam etching behavior is first studied on thin (1–5 L) MoS_2 flakes, which are deposited on SiO_2 surface through mechanical exfoliation. The number of layers of MoS_2 flake (1–5 L indicated in Fig. 1A) is confirmed by the optical contrast from an optical microscope (the inset of Fig. 1A), the height from atomic force microscopy (AFM) (Fig. S1) and Raman spectra (Fig. S2) [1,2]. The steam vapor is mixed with Ar carrier gas at ambient temperature and the gas mixture is then introduced into the hot furnace. The MoS_2 sample is exposed to the reacting gas at 500 °C for 30 min and 60 min which resulted in the surface morphologies of the MoS_2 flakes shown in Fig. 1B and C, respectively. Here, our AFM images show that a number of 1D nano-channels have been formed from the edge and inwards on the exposed basal planes of the MoS_2 flake. The uniform direction of the nano-channels implies that the steam vapor etching follows an anisotropic behavior. The etching process initiates at the MoS_2 perimeter and along certain crystallographic directions. No etching is observed when the temperature is below 500 °C (Fig. S3), suggesting that the present etching mechanism is different from that using the air exposure [25–28]. Interestingly, the high-resolution AFM images (Fig. 1D-K) also show that a nanoparticle with approximate size equal to the width of the nano-channel is located at the end position of each etched channel. Although the chemical nature of this nanoparticle is not determined, we speculate that it is molybdenum oxide formed from the reaction of MoS_2 with H_2O during etching [29]. The position of the nanoparticle at the reaction front of the etched channel indicates that it may serve as a catalyst steering and facilitating the etching process. The line-profiles in Fig. 1L show that the depth of the 1D nano-channel is 0.7 nm, in agreement with the thickness of one single-layer (SL) MoS_2. The widths of the nano-channels are widened after etching for additional 30 min (Fig. 1M), but the depth of the nano-channels remained unchanged. This phenomenon is also observed on another MoS_2 flake (see Fig. S5) meaning that the MoS_2 edge can also be etched without the help of molybdenum oxide nanoparticle. It should be notable that the etching speed with the help of molybdenum oxide nanoparticle (~ 25 nm/min, see Fig. 1O) is much higher than the etching speed without the help of molybdenum oxide nanoparticle (~ 1.2 nm/min, see Fig. S5) which clearly identify its role in the steam etching process. The relative orientation of the nano-channels along their growth direction within a single layer is separated by ± 60° degree in accordance with the six-fold symmetry of MoS_2. Furthermore, Fig. 1E and I and also Fig. 1N show that the nano-channels can change their direction during etching (see Figs. S5 and S6) while obeying the six-fold symmetry, which indicates that the etching mechanism follows the low-index crystallographic orientations of the MoS_2 lattice. The channel formation indicates an anisotropic etching behavior. This morphology is compatible with the preferential formation of low-energy edge terminations of MoS_2, referred to as either S-edges or Mo-edges, known to be particularly active in hydrogen evolution [3,30]. The etching speed is comparable for all layers of MoS_2 except 1 L MoS_2 (Fig. 1O), indicating that there is no obvious correlation between the etching speed and the thickness of the MoS_2. A noteworthy exception is that the area of 1 L is decreasing with speed of 5 nm/min, however, that no obvious channels are formed on 1 L MoS_2 during the etching process (Fig. 1F and J). The different etching behavior is evidently caused by a substrate effect. We speculate that a charged impurity on the SiO_2 substrate could pin the molybdenum oxide catalyst and thus impede the etching within the first layer [31]. Thus, we have demonstrated that MoS_2 can be etched by steam and form nanochannels on MoS_2 with crystalline edges, in a similar way as etching of graphene to form nanoribbon [32].

2.2. 2D steam vapor etching of MoS_2

A different etching morphology develops on the few layer MoS_2 sample (Fig. S7) and bulk MoS_2 (Fig. 2 and Fig. S8) when the

temperature increases further to 600 °C. Instead of nano-channels, small triangular pits are formed within the exposed basal planes of MoS_2, which can be attributed to anisotropic steam etching initiated at intrinsic structural defects. Compared with the sample produced at lower temperature etching, the nanoparticles that control the etching behaviors have disappeared. The time-resolved 2D etching (Fig. S9) directly proves that the steam etching follows a layer-by-layer etching behavior. The uniform orientation of the triangular pits and their single-layer (SL) height (Fig. 2B and C) indicates that the steam etching results in the formation of low-index edges embedded within the MoS_2 layer [25,26]. The single-layer triangular MoS_2 pits in Fig. 2D can in principle adopt two different low-index edge orientations, either S-edge or Mo-edge. All the triangular pits (Fig. 2A) have the same orientation within the same MoS_2 layer, indicating that the pits formed in the same MoS_2 layer have same edge configuration. However, we cannot determine the particular edge structure. From the cross section model obtained by removal of triangular patches from a single layer in Fig. 2D, the Mo atom on the Mo-edge $(10\bar{1}0)$ has unsaturated coordinated S atoms, comparing with the Mo atom on the S-edge $(\bar{1}010)$ which retains its coordination to size sulfur. The triangular pits observed in this study are assumed to be S-terminated edge [33,34], while there is some controversy. Fig. 2E and F show AFM images of the etched MoS_2 on different MoS_2 layers. The line profile (Fig. 2G) clearly reveals the height of the MoS_2 step and the depth of the triangular pits to be a single-layer. The triangular pits on adjacent layers show opposite orientations, but have the same S-edges (Fig. 2F) because the AB-stacking of bulk MoS_2 places the S atoms of the top layer above the Mo atoms of the underlying layer, equivalent to an alternating 60° rotation of in-plane crystallographic directions between layers. According to the schematic drawing in Fig. 2H, triangular pits with opposite orientation on adjacent layers therefore have the same edge termination.

2.3. 3D steam vapor etching of MoS_2

The MoS_2 surface morphology further develops when the etching temperature is increased to 700 °C. The resulting morphology now reflects tens-of-layers deep cavities with an apparent hexagonal outline as shown in Fig. 3A (and also see Fig. S10 and S11). A typical high-resolution AFM image of a hexagonal cavity (Fig. 3B) shows that the cavity is in fact composed of a larger triangular pit in the topmost layer which transitions into a hexagonal shape for deeper layers. The correlated line-profile (Fig. 3C) through the cavity directly demonstrates that the step height is always an even number of MoS_2 layers in vertical direction, except the topmost layer (1SL) and the bottommost layer (7SL) of the cavity. For the formation of the hexagonal cavity, firstly, a triangular pit with S-edge will be etched in the top MoS_2 layer (labeled as $E_{1\text{-}S}$) (Fig. 3D), and then a small triangular pit formed in the bottom MoS_2 layer with the same S-edges (Fig. 3E, labeled as $E_{2\text{-}S}$), where the pit orientation is opposite with the one formed in top layer. While the etching goes on, the $E_{2\text{-}S}$ edges will keep etching and the bottom triangular pit grows bigger, and finally stops (Fig. 3F). The etching of $E_{2\text{-}S}$ edges is then prevented by the top $E_{1\text{-}S}$ edges to form vertical (S-edge/Mo-edge, $E_{1\text{-}S}/E_{2\text{-}Mo}$ as labeled in Fig. 3G) structures. Thus, the hexagonal pit on second layer will initiate the etching behavior to form deeper 3D pit with new structures (in-plane hexagonal pit with alternated S-edges and Mo-edges; out-of-plane with S-edge/Mo-edge unit). The hexagonal cavity morphology arises due to the 2H-stacking sequence of MoS_2 indicating that Mo- and S-edge are aligned alternately. The alternating edge termination of a complete 3D MoS_2 cavity is illustrated in Fig. 3h, which is drawn according to the Fig. 3C. The detailed discussion of the edge sequence of the hexagonal cavity is shown in Section S1. In order to shed light on the detailed 3D steam etching mechanism, time-resolved AFM was performed on MoS_2 flakes, as shown in Fig. S12. Interestingly, the etching direction primarily goes towards into the surface at this temperature, which is different from the etching direction of 2D layer-by-layer etching. To further reveal the direction of the etched MoS_2 edges, we recorded the atomic structure on the basal plane by lateral force microscopy as shown in Fig. S13. It can be clearly seen that the edges on etch pit are parallel to the close packed directions on the MoS_2 basal plane, showing that the edges must be either the Mo or S edges. Significantly, the atomic resolution images recorded from four neighbor layers have the identical FFT patterns, which suggest that the etched edges on different layers have the same zigzag configuration. Comparing with other chemical etching, such as O_2 and H_2 [22–24], the etching behavior on MoS_2 by H_2O steam vapor is fairly sensitive to temperature, which allows to create 1D nanochannels, 2D in-plane triangular pits and 3D vertical hexagonal cavities nanoscale morphology by varying the etching temperature (per ~ 100 °C).

2.4. In-situ TEM imaging of etching MoS_2

The AFM results show that steam etching of MoS_2 flakes in the range from 500 to 700 °C can be used to selectively control the formation of three widely different surface morphologies, which however share the property that new active edges are created. The resulting morphologies in the temperature range reflect a complex interplay between preferential etching along low-index crystallographic directions in MoS_2 and mobility of vacancies, which leads to equilibrium shapes formed within the MoS_2 layers. We further explored steam etching of MoS_2 nanoparticles by means of *in-situ* transmission electron microscopy (TEM). The MoS_2 were synthesized in the microscope by thermally decomposing ammonium heptamolybdate ($(NH_4)_6Mo_7O_{24}$) to produce MoO_2 nanoparticles, which were subsequently sulfided in the microscope. The resulting nanoparticle shells consisted of concentric MoS_2 layers with a core of reminiscent molybdenum oxide, resembling the fullerene-like multi-layer MoS_2 nanostructures previously reported by Tenne et al. [35]. Fig. 4A shows that the as-prepared nanoparticles expose mainly the MoS_2 (002) basal plane reflecting a low availability of edge sites so such structures are expected to be poor HER catalysts. However, edge sites can be formed in these layers by exposure to steam at elevated temperatures. The steam etching was monitored by acquisition of a time-resolved series of TEM images of the MoS_2 nanostructures *in situ* during exposure to 1 mbar of H_2O at 700 °C. Fig. 4B-D show that etching initiates at the outer MoS_2 layer (Fig. 4B) by removal of part of the MoS_2 layer, so that a pair of edge appears in the projected images (Fig. 4B). Thus, these observations show that the steam etching is a viable method to sculpture surface morphology of nanomaterials with curved MoS_2 layers as well and therefore offers a way to increase the abundance of edge sites in MoS_2 materials of relevance for heterogeneous catalysis.

2.5. Hydrogen evolution on MoS_2 basal plane

We quantify the enhancement effect of the HER activity associated with the multiplication of active sites on the steam etched MoS_2 flakes. The sample is etched at 700 °C, and its surface is further checked by AFM before device fabrication. The HER activity is investigated using a three-electrode configuration with Pt wire as the counter electrode, micro Ag/AgCl electrode as the reference electrode, and one gold pad connecting with the single individual MoS_2 flake as the working electrode, as shown in Fig. 5A and B. The sample except for the MoS_2 basal plane is fully covered by PMMA to ensure that the measured activity originates only from the exposed area (white-dashed square in Fig. 5C). The exposed window on the MoS_2 basal plane is prepared by electron-beam lithography (see Experimental section). Typical polarization curves are measured in the microcell configuration on pristine and etched MoS_2, respectively, as shown in Fig. 5D. It can be seen that the onset potential is 492 mV at a current density of 5 mA/cm^2 for the pristine sample whereas the onset potential drops to 316 mV for etched MoS_2 sample. The electrochemical measurement implies that the same current density can be obtained at a much lower potential after steam

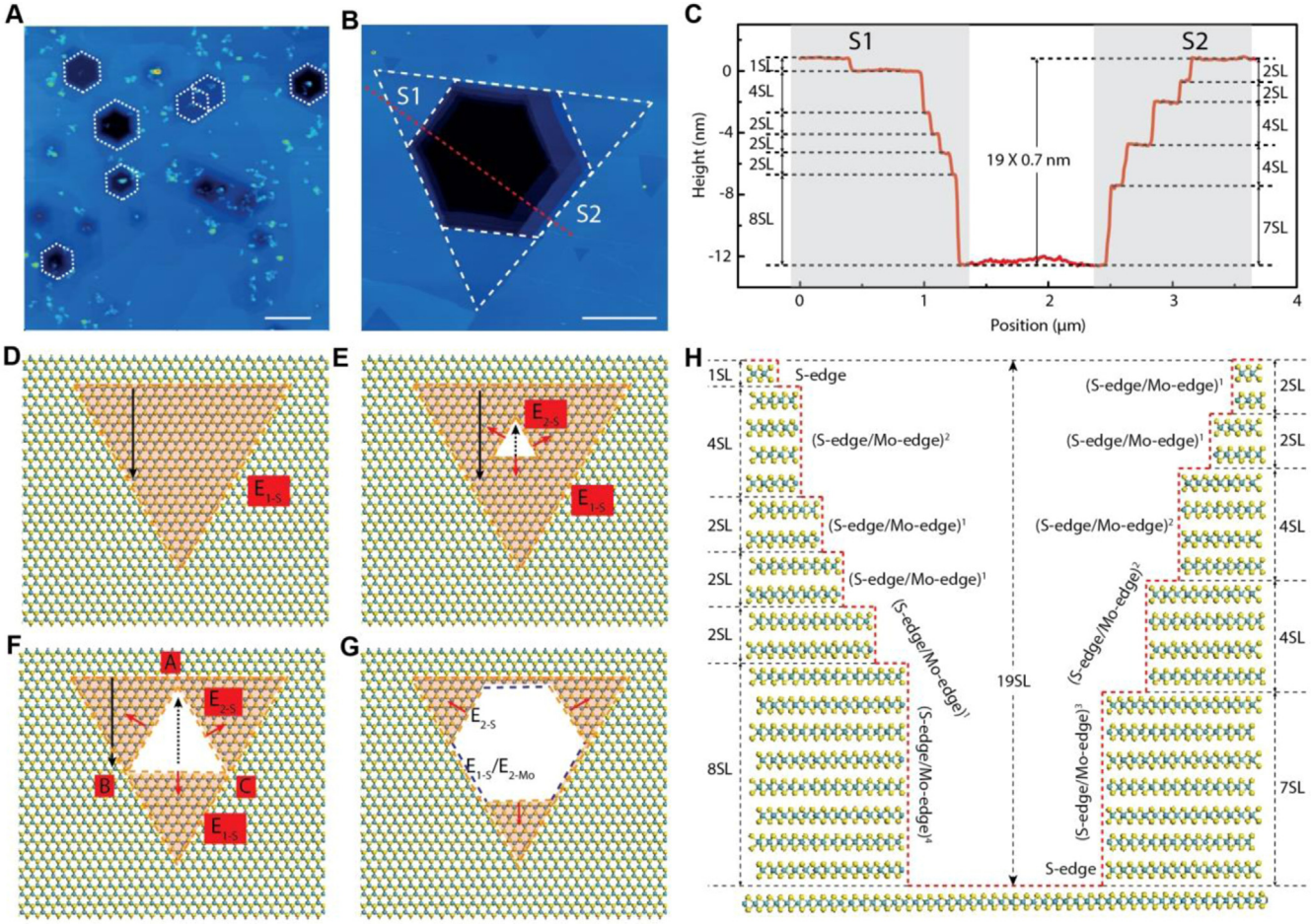

Fig. 3. 3D steam vapor etching of MoS_2. (**A**) A typical AFM image of bulk MoS_2 after steam etching for 30 min at 700 °C. (**B**) A typical high-resolution AFM image of the out-of-plane cavity. (**C**) Line-profile corresponding to the dashed red line marked in (B). (**D-G**) The schematic drawing evolution to form hexagonal pits on two layers MoS_2. (**H**) The schematic drawing the section according to (C). The scale bars in (A) and (B) are 1 μm. (For interpretation of the references to color in this figure legend, the reader is referred to the web version of this article.)

etching. It is noticed that platinum counter electrode may give influence on the polarization curve after cycling voltammetric sweeping with large scanning speed (hundreds mV/s) [36]. By reducing the scanning speed and the number of cycle, the platinum contamination can be dramatically reduced. In this work, the polarization curve is obtained with very low scanning speed (5 mV/s). The AFM image and EDS spectrum of the MoS_2 flake after hydrogen evolution reaction (see Fig. S15) indicate that no detectable platinum particle is formed confirming the electrochemical polarization current is originating from the catalytic property of MoS_2 itself. Meanwhile, the corresponding Tafel

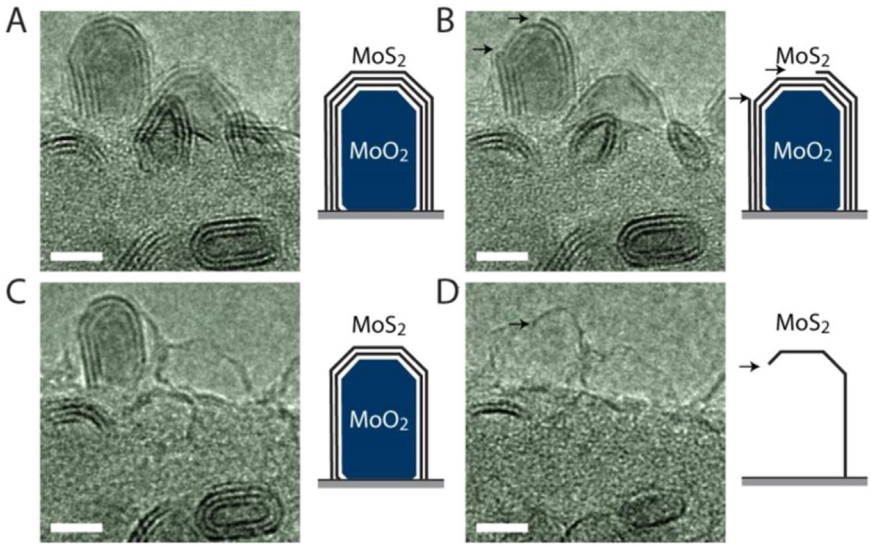

Fig. 4. Time-resolved *in-situ* TEM imaging of MoS_2 during exposure to steam. (**A**) TEM image and sketch of as-prepared MoO_2:MoS_2 nanoparticles. (**B-D**) Time-resolved TEM images of the MoS_2 nanoparticles after 7 min (B), 12 min (C) and 17 min (D) exposure to 1 mbar of H_2O at 700 °C. Sketches are included to guide the eye pinpointing the steam-induced edge formation. The scale bars are 5 nm. The role of electron illumination is shown in Fig. S14.

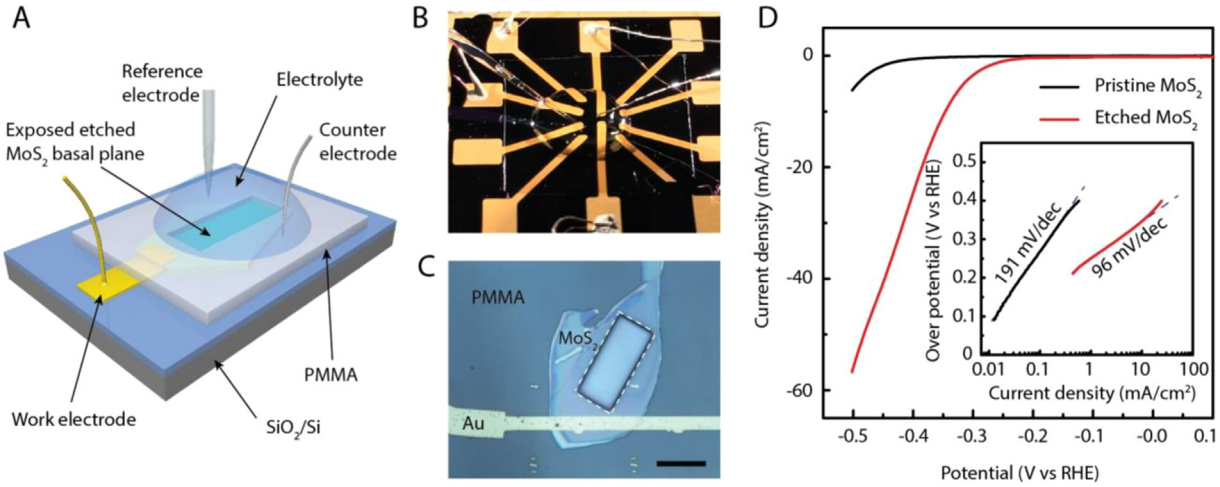

Fig. 5. Hydrogen evolution measurements on pristine and etched MoS_2 basal plane. (**A**) Schematic of the setup showing a single gold pad connected with a MoS_2 flake used as the working electrode. Pt wire and micro Ag/AgCl electrodes are used as counter and reference electrode, respectively. The whole sample is covered with PMMA except a window on the MoS_2 basal plane to ensure that the activity is only originating from the exposed area. (**B**) Photography of the electrochemical microcell. (**C**) Optical microscope image of the microcell where a window (white-dashed square) was exposed on MoS_2 basal plane. The scale bar is 20 μm. (**D**) The typical polarization curves measured from pristine and etched MoS_2 based microcell in 0.5 M H_2SO_4 with scan ratio of 5 mV/s, and the inset is the corresponded Tafel plot.

plots are shown inset in Fig. 5D, showing a 49.7% decrease of the Tafel slope (from 191 mV/dec to 96 mV/dec), indicating an enhanced catalytic activity [8,9,22,37–39]. A previous study demonstrates the influence of contact resistance on electrochemical performance [11]. To eliminate the contact resistance influence, many four-terminated devices on pristine and etched MoS_2 flakes are fabricated, and the contact resistances are evaluated, as shown in Fig. S16. The contact resistance on pristine and etched MoS_2 flakes are similar with each other in the range from 10^{-1} to 10^{0} kΩ mm, which is much lower than the critical contact resistance (10^{1} to 10^{2} kΩ mm) indicating that the enhanced catalytic activity is originated from the etched edges rather than the variation of contact resistance [11]. The introduced edges by steam etching are able to modulate its surface structure and thus change the electronic properties of the surface, which allow tuning the reaction barriers effectively [40]. A smaller Tafel slope indicates a faster increase of the HER rate with the decrease of over-potential. Three steps (discharge, combination and desorption steps) have been proposed for converting H^+ to H_2 on the catalyst surface, in which the first discharge step

$$H_3O^+ + e^- + MoS_2\text{-edge} \rightarrow MoS_2\text{-edge-H} + H_2O$$

is the key rate-determining step when the Tafel slop is higher than 120 mV/dec [8,9,22,37–39]. In this study, the observed 191 mV/dec Tafel slop on pristine MoS_2 flake is even higher than CVD-grown MoS_2 (150–160 mV/dec), which may be attributed to that the CVD-grown MoS_2 has some S vacancy in CVD-grown MoS_2 [9,22]. The higher Tafel slope in our case show that the proton transfer in the discharge step is the limiting step resulting from its very low abundance of edge sites [38]. In steam-etched MoS_2 flake, the free energy barrier of the discharge step is reduced to be comparable with that of the following desorption or combination step, resulting in a significant drop of the slope to 96 mV/dec. The improved Tafel slope originates from the generated MoS_2-edges on MoS_2 basal plane which will effectively decrease the activation energy [8,9]. Each surface structure (edges, corners, steps and kinks) may be able to modulate its surface structure and thus change the electronic properties of the surface, which may tune the reaction barriers effectively [40]. Thus, the improved performance should be attributed to the creation of fresh cavities with huge amounts of edges, corners and steps after etching.

2.6. DFT calculations on etched MoS_2

The electrocatalytic splitting of water by the microcell technique quantitatively demonstrates the enhanced catalytic activity of etched MoS_2, suggesting that steam vapor etching is a promising candidate method to improve catalyst performance. The interesting MoS_2 nanostructures etched by steam vapor etching will expose both Mo edges, which were previously concluded to be active in HER and S edges [30]. To obtain fundamental insights on the potential activity of the etched S-edges in the electrocatalytic reaction, we employed density functional theory (DFT) calculations to investigate the adsorption free energy of H atoms (ΔG_{H^*}) at different sites of the S-edge terminated etched triangle in the MoS_2 model structures as shown in Fig. 6. ΔG_{H^*} has been widely considered to be a useful indicator for the catalytic activity and a ΔG_{H^*} value close to zero generally suggests high catalytic activity [29,41]. Here, a positive ΔG_{H^*} suggests the hydrogen form a strong bond to the catalyst, and the negative ΔG_{H^*} implies no efficient bonding to the catalyst. Both of them will lead to inefficient hydrogen release and proton–electron transfer resulting in the decreasing of catalytic activity. As shown in Fig. 6B, the ΔG_{H^*} for basal plane sites on pristine MoS_2 is 1.24 eV, indicating its inertness, in line with previous simulations [42]. Significantly, one can see that the ΔG_{H^*} for etched MoS_2 decrease to − 0.48 eV, which indicates bonding of H with a value much closer to zero compared to pristine MoS_2. Furthermore, the site dependence of ΔG_{H^*} on etched MoS_2 are shown in Fig. 6C and the adsorption site is shown in Fig. S17. As can be seen, along the etched edge from P2 (− 0.74 eV) to P6 (− 0.61 eV), ΔG_{H*} has no obvious change, but always closer to zero compared to pristine MoS_2, suggesting the etched edge itself is active. ΔG_{H^*} values on S atoms at the corner (P1) is + 1.17 eV, suggesting no hydrogen adsorption at the corner of the MoS_2 pit. Moreover, away from the etched edge (P7 to P10), the ΔG_{H^*} will increase from + 0.59 eV (P7) to + 1.11 eV (P10), which is still better than ΔG_{H^*} of pristine MoS_2. It should be noted that the ΔG_{H^*} will increase and tend to the value of pristine MoS_2. This suggests that the etched pit not only active the etched edge, but also active the nearby area, attributing to the modulated electronic structure.

In addition, electronic structure calculation is performed to analyze origin of the site dependence of ΔG_{H^*} on etched MoS_2 because the catalytic property of a catalyst is determined fundamentally by its

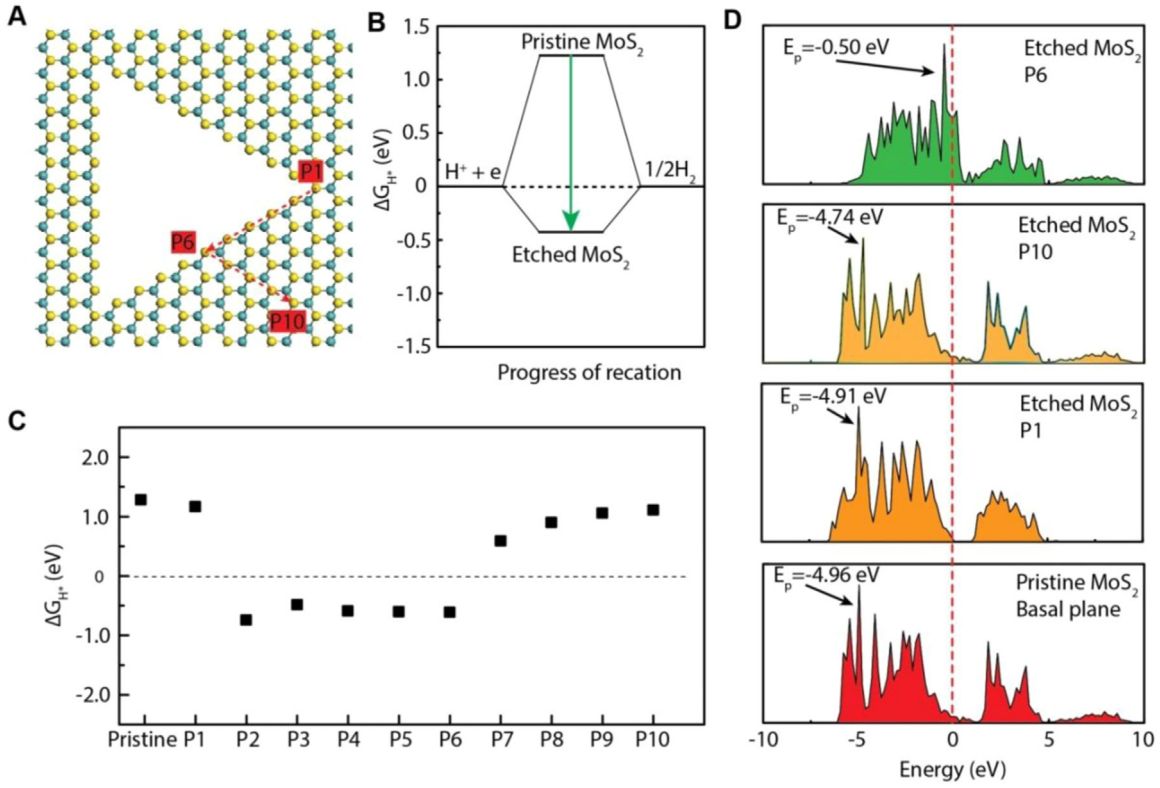

Fig. 6. DFT calculation on etched MoS_2. (**A**) The etched MoS_2 model, where the hydrogen atom is adsorbed on different sites. (**B**) The free energy diagrams for pristine and etched MoS_2. (**C**) The HER free energy for different hydrogen atom adsorbed sites. (**D**) Projected density of states (PDOS) plots of 2p orbitals for S atom on basal plane and P1, P6 and P10 adsorption sites of etched MoS_2. The red dash line represents the Fermi level. (For interpretation of the references to color in this figure legend, the reader is referred to the web version of this article.)

electronic structure [40]. The most commonly related electronic band structure is the valence band, and the higher the valence band position (E_p) indicates a stronger the H* adsorption strength [43,44]. Therefore, the projected density of states (PDOS) of various active sites (P1-P10 and basal plan) were calculated illustrating in Fig. 6D. As seen, E_p for S atom on the etched edge (P6) is − 0.50 eV, which is much larger than that of E_p for S atom on the basal plane (− 4.96 eV). The higher energy level of E_p suggests a higher energy level of the anti-bonding states and a lower occupancy, which will induce a stronger interaction between adsorbed hydrogen atom and catalyst site (S atom) [43,44]. Therefore, the highest energy level for P6 means the strongest adsorption of hydrogen and lowest values of ΔG_{H^*}. Moreover, the E_p for S atom is − 4.91 eV and − 4.71 eV, corresponding to S atom on P1 (corner) and P10 (away from edge), respectively. The higher energy level of P1 and P10 compared with that on basal plane indicates a well adsorption and an improved ΔG_{H^*}.

3. Conclusion

In summary, a simple and environmentally friendly steam treatment method has been developed with the demonstrated ability to create various densities of active edge sites on the inert basal planes of MoS_2. Different edge morphologies, represented by 1D nano-channel, 2D in-plane triangular pit and 3D out-of-plane cavity surface structures could be created through controlling the etching temperature during the steam etching process. A high amount of created active edges on MoS_2 basal plane effectively decrease its surface free energy barrier and improve its catalytic activity, which is quantitatively studied by fabricating an electrochemical microcell containing steam etched single MoS_2 flakes. Thus steam etching offers a straightforward and general process to nanoengineer pristine MoS_2 materials for enhanced catalytic operation.

4. Experimental section

4.1. Sample preparation and steam vapor etching of MoS_2

Few-layer MoS_2 flakes were deposited on the Si substrate with a 300 nm SiO_2 film by mechanical exfoliation of bulk MoS_2 crystal. Both bulk MoS_2 and transfered few-layered MoS_2 were then placed in a quartz tube, where highly purified Ar (1000 sccm) was flowed for 30 min to exclude the effect of air. After that, the MoS_2 samples were then annealed at different temperatures in water steam, which was carrier into the quartz tube by Ar (500 sccm). During the whole etching process, the total pressure was kept at atmospheric pressure and water steam is assumed to be present at its vapor pressure at room temperature (~ 23 mbar). When the etching process finished, the MoS_2 samples were cooled to room temperature and taken out for analysis.

4.2. Raman and AFM characterizations

The Raman spectroscopy experiments were carried out with 514 nm and 1.0 mW laser excitation (Renishaw inVia Raman Spectroscope, Sweden). All AFM images were captured by a commercial Dimension Icon AFM (Bruker, Santa Barbara, USA) in tapping mode with ultrasharp probes (OMCL-AC160TS-C2, Olympus, Japan) in air. Analysis of AFM images was done with Scanning Probe Image Processor software (SPIP™, Image Metrology ApS, Lyngby, Denmark). The atomic resolution edge configuration was investigated by lateral force microscopy, which is conducted on MultiMode-8 with soft probes (MSNL-10, 0.6 N/m).

4.3. Transmission electron microscopy of steam-etching of MoS_2 nanoparticles

The experiments have been performed using a Philips/FEI Company

CM300 FEG-ST transmission electron microscope equipped with a differential pumping system [45]. In the experiments, ammonium heptamolybdate, $(NH_4)_6Mo_7O_{24}$ was loaded onto a FEI NanoEx heating device and heated in the microscope base vacuum to decompose the precursor into MoO_2 nanoparticles [46]. The MoO_2 was subsequently sulfided by exposure to 1 mbar of 10% H_2S in H_2 at 700 °C for 40 min followed by 800 °C for 35 min in the electron microscope. For steam etching, the MoS_2 nanostructures were exposed to 1 mbar of H_2O. Prior to vapor exposing the sample, the water was cleaned by successive freeze–pump-thaw cycles of the water container until contaminants were absent in mass spectrometry of the gas in the container. The mass spectrometer was mounted on the second differential pumping stage of the electron microscope [45]. To monitor the MoS_2 nanostructures during steam exposure, the microscope was operated at a primary energy of 300 keV and at an electron dose rate of 150 electrons $Å^{-2}\,s^{-1}$. Images were acquired with a charged coupled device (CCD) camera (Tietz F114) with the projection system of the microscope corresponding to an effective pixel size of 0.07 nm. At each time step and position, a series of 5 successive images was acquired with a CCD exposure time of 1 s. The images in each series were post-aligned using cross-correlation and summed to a final image with improved signal-to-noise ratio. The final images are represented as a direct representation of the CCD current output in a monochromatic green color scale. Additionally, the image contrast and brightness have been linearly adjusted.

4.4. Single MoS_2 flake based microcell fabrication and electrocatalytic hydrogen evolution reaction

MoS_2 flakes were prepared on SiO_2/Si by mechanical exfoliation, and further treated at 700 °C in steam. After further check of the etched pattern by AFM, poly(methyl methacrylate) (PMMA) were spin-coated on its surface and then baked at 100 °C for 5 min. Then a knife was used to cut the PMMA with small pieces with the etched MoS_2 flake is inside. The small PMMA/MoS_2 pieces could be quickly released by immerse in 1% HF solution. After washing them several times in DI water, the small PMMA/MoS_2 pieces were transferred to the center of the new SiO_2/Si substrate which has been deposited with 10 gold contact pads via metal mask. The small piece makes it easy to place at the correct site at the center before drying. After a bake at 150 °C for 5 min, the PMMA could be removed by warm acetone. A new PMMA layer was spin-coated on the sample at 4000 rpm and then baked at 180 °C for 2 min. Electron-beam lithography was employed to design microelectrodes patterns to connect the MoS_2 flake with the closed contact pads. Each contact pad is connected to only one MoS_2 flake and thus each flake can be tested separately. Once the MoS_2 flakes were connected, a second electron-beam lithography process was employed to expose the basal plane of MoS_2 and cover the edges of MoS_2 flake and the electrodes. To fully cover them, PMMA A11 was spin-coated on the sample at 4000 rpm for 60 s, and baked at 180 °C for 5 min. Its thickness is about 2 μm. And then, to eliminate the charge effect, conductive polymer was spin-coated on it at 2000 rpm for 60 s and baked at 90 °C for 2 min. The window was opened on the MoS_2 flake by e-beam lithography with 300 $\mu C/cm^2$ dose. More attention was devoted to make sure that no gold and none of the original edges of MoS_2 flakes were be exposed to the electrolyte.

After the sample was baked at 180 °C for 10 min, the HER measurement was performed. Linear sweep voltammetry with a scan rate of 5 mV/s was conducted in 0.5 M H_2SO_4 solution using a Pt wire as the counter electrode. The micro reference electrode was calibrated for the reversible hydrogen potential, where E(vs RHE) = E(vs Ag/AgCl) + 0.197 V. Before measurement, H_2SO_4 solution was degassed using pure Ar gas.

4.5. Computational details and models

Geometry optimization, total energy calculations and electronic structure were performed by using first-principle calculations within the framework of density functional theory (DFT), as implemented in the plane wave set Vienna ab initio Simulation Package (VASP) code. The Perdew-Burke-Ernzerhof (PBE) functional within the generalized gradient approximation (GGA-PBE) was used to model exchange correlation energy. The projector augmented wave (PAW) pseudo-potentials were used to describe the interaction valence electron and ionic cores. The kinetic energy of 500 eV cut off was set in all calculations. A Gaussian smearing with $\sigma = 0.05$ eV to the orbital occupation is applied to broaden the Fermi level for accurate electronic convergence, whilst a tetrahedron method with Blöchl corrections was employed for the accurate electronic structure calculations. To simulate pristine and etched MoS_2, a $12 \times 12 \times 1$ supercell was used and a vacuum slab of 10 Å was inserted in z direction to prevent interaction between two neighboring surfaces. Geometry optimizations were performed by using the BFGS algorithm with a $1 \times 1 \times 1$ k-mesh until the maximum force component of the system converges to 0.02 eV/Å, while a $2 \times 2 \times 1$ k-mesh is adopted for total energy and electronic structure calculations. The adsorption free energy of hydrogen, ΔG_{H^*}, is a good descriptor to estimate the activity of hydrogen evolution reaction, which is determined in the formula: $\Delta G_{H^*} = \Delta E_{H^*} + \Delta E_{ZPE} - T\Delta S$ [29,47]. In the formula, $\Delta E_{H^*} = E_{(surface+H^*)} - E_{surface} - 1/2E_{H2}$, where $E_{(surface+H^*)}$ and $E_{surface}$ are total energy of the surface model with and without H* adsorption, respectively. E_{H2} is the energy of a single H_2 molecule isolated in vacuum. ΔE_{ZPE} is the zero-point energy difference between the adsorbed state of the system and the gas phase state. ΔS_H is the entropy difference between the adsorbed state of the system and the gas phase standard state.

Acknowledgements

This research was supported by grants from the Danish National Research Foundation (Grant no. DFF-6108-00396), Young Investigator Program from the Villum Foundation (Grant no. VKR022954), AUFF NOVA-Project (Grant no. AUFF-E-2015-FLS-9-18), EU H2020 (MNR4SCELL no. 734174) and The National Natural Science Foundation of China (Grant nos. 51372033 and 21528501), the National High Technology Research and Development Program of China (Grant no. 2015AA034202). STH, CDP and JVL acknowledge funding from Innovation Fund Denmark (CAT-C no. 12-132681). We also thank J. Kibsgaard for the useful discussion on the electrochemical measurement.

Appendix A. Supporting information

Supplementary data associated with this article can be found in the online version at http://dx.doi.org/10.1016/j.nanoen.2018.04.067.

References

[1] M. Chhowalla, H.S. Shin, G. Eda, L.-J. Li, K.P. Loh, H. Zhang, The chemistry of two-dimensional layered transition metal dichalcogenide nanosheets, Nat. Chem. 5 (2013) 263–275.
[2] H.T. Wang, H.T. Yuan, S.S. Hong, Y.B. Li, Y. Cui, Physical and chemical tuning of two-dimensional transition metal dichalcogenides, Chem. Soc. Rev. 44 (2015) 2664–2680.
[3] T.F. Jaramillo, K.P. Jorgensen, J. Bonde, J.H. Nielsen, S. Horch, I. Chorkendorff, Identification of active edge sites for electrochemical H_2 evolution from MoS_2 nanocatalysts, Science 317 (2007) 100–102.
[4] C.C. Cheng, A.Y. Lu, C.C. Tseng, X. Yang, M.N. Hedhili, M.C. Chen, K.H. Wei, L.J. Li, Activating basal-plane activity of two-dimensional MoS_2 monolayer with remote hydrogen plasma, Nano Energy 30 (2016) 846–852.
[5] H.I. Karunadasa, E. Montalvo, Y.J. Sun, M. Majda, J.R. Long, C.J. Chang, A molecular MoS_2 edge site mimic for catalytic hydrogen generation, Science 335 (2012) 698–702.

[6] Y.-R. An, X.-L. Fan, Z.-F. Luo, W.-M. Lau, Nanopolygons of monolayer MoS_2: best morphology and size for HER catalysis, Nano Lett. 17 (2017) 368–376.
[7] J.D. Benck, T.R. Hellstern, J. Kibsgaard, P. Chakthranont, T.F. Jaramillo, Catalyzing the hydrogen evolution reaction (HER) with molybdenum sulfide nanomaterials, ACS Catal. 4 (2014) 3957–3971.
[8] J.F. Xie, H. Zhang, S. Li, R.X. Wang, X. Sun, M. Zhou, J.F. Zhou, X.W. Lou, Y. Xie, Defect-rich MoS_2 ultrathin nanosheets with additional active edge sites for enhanced electrocatalytic hydrogen evolution, Adv. Mater. 25 (2013) 5807–5813.
[9] H. Li, C. Tsai, A.L. Koh, L. Cai, A.W. Contryman, A.H. Fragapane, J. Zhao, H.S. Han, H.C. Manoharan, F. Abild-Pedersen, J.K. Norskov, X. Zheng, Activating and optimizing MoS_2 basal planes for hydrogen evolution through the formation of strained sulphur vacancies, Nat. Mater. 15 (2016) 48–53.
[10] C. Tsai, F. Abild-Pedersen, J.K. Nørskov, Tuning the MoS_2 edge-site activity for hydrogen evolution via support interactions, Nano Lett. 14 (2014) 1381–1387.
[11] D. Voiry, R. Fullon, J. Yang, C. de Carvalho Castro e Silva, R. Kappera, I. Bozkurt, D. Kaplan, M.J. Lagos, P.E. Batson, G. Gupta, A.D. Mohite, L. Dong, D. Er, V.B. Shenoy, T. Asefa, M. Chhowalla, The role of electronic coupling between substrate and 2D MoS_2 nanosheets in electrocatalytic production of hydrogen, Nat. Mater. 15 (2016) 1003–1009.
[12] H. Li, M. Du, M.J. Mleczko, A.L. Koh, Y. Nishi, E. Pop, A.J. Bard, X. Zheng, Kinetic study of hydrogen evolution reaction over strained MoS_2 with sulfur vacancies using scanning electrochemical microscopy, J. Am. Chem. Soc. 138 (2016) 5123–5129.
[13] R. Kappera, D. Voiry, S.E. Yalcin, B. Branch, G. Gupta, A.D. Mohite, M. Chhowalla, Phase-engineered low-resistance contacts for ultrathin MoS_2 transistors, Nat. Mater. 13 (2014) 1128–1134.
[14] X.M. Geng, W.W. Sun, W. Wu, B. Chen, A. Al-Hilo, M. Benamara, H.L. Zhu, F. Watanabe, J.B. Cui, T.P. Chen, Pure and stable metallic phase molybdenum disulfide nanosheets for hydrogen evolution reaction, Nat. Commun. 7 (2016) 10672.
[15] B. Zhang, J. Liu, J. Wang, Y. Ruan, X. Ji, K. Xu, C. Chen, H. Wan, L. Miao, J. Jiang, Interface engineering: the $Ni(OH)_2/MoS_2$ heterostructure for highly efficient alkaline hydrogen evolution, Nano Energy 37 (2017) 74–80.
[16] J. Kibsgaard, Z. Chen, B.N. Reinecke, T.F. Jaramillo, Engineering the surface structure of MoS_2 to preferentially expose active edge sites for electrocatalysis, Nat. Mater. 11 (2012) 963–969.
[17] Y.H. Chang, C.T. Lin, T.Y. Chen, C.L. Hsu, Y.H. Lee, W.J. Zhang, K.H. Wei, L.J. Li, Highly efficient electrocatalytic hydrogen production by MoS_x grown on graphene-protected 3D Ni foams, Adv. Mater. 25 (2013) 756–760.
[18] X. Hai, W. Zhou, S. Wang, H. Pang, K. Chang, F. Ichihara, J. Ye, Rational design of freestanding MoS_2 monolayers for hydrogen evolution reaction, Nano Energy 39 (2017) 409–417.
[19] Y.W. Zhu, S. Murali, M.D. Stoller, K.J. Ganesh, W.W. Cai, P.J. Ferreira, A. Pirkle, R.M. Wallace, K.A. Cychosz, M. Thommes, D. Su, E.A. Stach, R.S. Ruoff, Carbon-based supercapacitors produced by activation of graphene, Science 332 (2011) 1537–1541.
[20] J.W. Bai, X. Zhong, S. Jiang, Y. Huang, X.F. Duan, Graphene nanomesh, Nat. Nanotechnol. 5 (2010) 190–194.
[21] T.H. Han, Y.-K. Huang, A.T.L. Tan, V.P. Dravid, J. Huang, Steam etched porous graphene oxide network for chemical sensing, J. Am. Chem. Soc. 133 (2011) 15264–15267.
[22] G. Ye, Y. Gong, J. Lin, B. Li, Y. He, S.T. Pantelides, W. Zhou, R. Vajtai, P.M. Ajayan, Defects engineered monolayer MoS_2 for improved hydrogen evolution reaction, Nano Lett. 16 (2016) 1097–1103.
[23] Y. Huang, J. Wu, X. Xu, Y. Ho, G. Ni, Q. Zou, G.K.W. Koon, W. Zhao, A.H. Castro Neto, G. Eda, C. Shen, B. Özyilmaz, An innovative way of etching MoS_2: characterization and mechanistic investigation, Nano Res. 6 (2013) 200–207.
[24] M.H. Jeon, C. Ahn, H. Kim, K.N. Kim, T.Z. LiN, H. Qin, Y. Kim, S. Lee, T. Kim, G.Y. Yeom, Controlled MoS_2 layer etching using CF_4 plasma, Nanotechnology 26 (2015).
[25] H. Zhou, F. Yu, Y. Liu, X. Zou, C. Cong, C. Qiu, T. Yu, Z. Yan, X. Shen, L. Sun, B.I. Yakobson, J.M. Tour, Thickness-dependent patterning of MoS_2 sheets with well-oriented triangular pits by heating in air, Nano Res. 6 (2013) 703–711.
[26] M. Yamamoto, T.L. Einstein, M.S. Fuhrer, W.G. Cullen, Anisotropic etching of atomically thin MoS_2, J. Phys. Chem. C 117 (2013) 25643–25649.
[27] J. Wu, H. Li, Z.Y. Yin, H. Li, J.Q. Liu, X.H. Cao, Q. Zhang, H. Zhang, Layer thinning and etching of mechanically exfoliated MoS_2 nanosheets by thermal annealing in air, Small 9 (2013) 3314–3319.
[28] R. Ionescu, A. George, I. Ruiz, Z. Favors, Z. Mutlu, C. Liu, K. Ahmed, R. Wu, J.S. Jeong, L. Zavala, K.A. Mkhoyan, M. Ozkan, C.S. Ozkan, Oxygen etching of thick MoS_2 films, Chem. Commun. 50 (2014) 11226–11229.
[29] E. Blanco, H.Y. Sohn, G. Han, K.Y. Hakobyan, The kinetics of oxidation of molybdenite concentrate by water vapor, Metall. Mater. Trans. B 38 (2007) 689–693.
[30] B. Hinnemann, P.G. Moses, J. Bonde, K.P. Jørgensen, J.H. Nielsen, S. Horch, I. Chorkendorff, J.K. Nørskov, Biomimetic hydrogen evolution: MoS_2 nanoparticles as catalyst for hydrogen evolution, J. Am. Chem. Soc. 127 (2005) 5308–5309.
[31] L. Liu, S. Ryu, M.R. Tomasik, E. Stolyarova, N. Jung, M.S. Hybertsen, M.L. Steigerwald, L.E. Brus, G.W. Flynn, Graphene oxidation: thickness-dependent etching and strong chemical doping, Nano Lett. 8 (2008) 1965–1970.
[32] L.C. Campos, V.R. Manfrinato, J.D. Sanchez-Yamagishi, J. Kong, P. Jarillo-Herrero, Anisotropic etching and nanoribbon formation in single-layer graphene, Nano Lett. 9 (2009) 2600–2604.
[33] M.V. Bollinger, K.W. Jacobsen, J.K. Nørskov, Atomic and electronic structure of MoS_2 nanoparticles, Phys. Rev. B 67 (2003) 085410.
[34] J.V. Lauritsen, J. Kibsgaard, S. Helveg, H. Topsoe, B.S. Clausen, E. Laegsgaard, F. Besenbacher, Size-dependent structure of MoS_2 nanocrystals, Nat. Nanotechnol. 2 (2007) 53–58.
[35] Y. Feldman, E. Wasserman, D.J. Srolovitz, R. Tenne, High-rate, gas-phase growth of MoS_2 nested inorganic fullerens and nanotubes, Science 267 (1995) 222–225.
[36] R. Chen, C. Yang, W. Cai, H.-Y. Wang, J. Miao, L. Zhang, S. Chen, B. Liu, Use of platinum as the counter electrode to study the activity of nonprecious metal catalysts for the hydrogen evolution reaction, ACS Energy Lett. 2 (2017) 1070–1075.
[37] H. Wang, D. Kong, P. Johanes, J.J. Cha, G. Zheng, K. Yan, N. Liu, Y. Cui, $MoSe_2$ and WSe_2 nanofilms with vertically aligned molecular layers on curved and rough surfaces, Nano Lett. 13 (2013) 3426–3433.
[38] D. Merki, X.L. Hu, Recent developments of molybdenum and tungsten sulfides as hydrogen evolution catalysts, Energy Environ. Sci. 4 (2011) 3878–3888.
[39] Z. Wang, Q. Li, F. Besenbacher, M. Dong, Facile synthesis of single crystal $PtSe_2$ nanosheets for nanoscale electronics, Adv. Mater. 28 (2016) 10224–10229.
[40] J.K. Norskov, T. Bligaard, J. Rossmeisl, C.H. Christensen, Towards the computational design of solid catalysts, Nat. Chem. 1 (2009) 37–46.
[41] M.-R. Gao, M.K.Y. Chan, Y. Sun, Edge-terminated molybdenum disulfide with a 9.4-Å interlayer spacing for electrochemical hydrogen production, Nat. Commun. 6 (2015) 7493.
[42] G. Li, D. Zhang, Q. Qiao, Y. Yu, D. Peterson, A. Zafar, R. Kumar, S. Curtarolo, F. Hunte, S. Shannon, Y. Zhu, W. Yang, L. Cao, All the catalytic active sites of MoS_2 for hydrogen evolution, J. Am. Chem. Soc. 138 (2016) 16632–16638.
[43] Y. Jiao, Y. Zheng, K. Davey, S.-Z. Qiao, Activity origin and catalyst design principles for electrocatalytic hydrogen evolution on heteroatom-doped graphene, Nat. Energy 1 (2016) 16130.
[44] A. Vojvodic, J.K. Norskov, Optimizing perovskites for the water-splitting reaction, Science 334 (2011) 1355–1356.
[45] P.L. Hansen, S. Helveg, A.K. Datye, Atomic-scale imaging of supported metal nanocluster catalysts in the working state, Adv. Catal. 50 (2006) 77–95.
[46] J. Wienold, Rolf E. Jentoft, T. Ressler, Structural investigation of the thermal decomposition of ammonium heptamolybdate by in situ XAFS and XRD, Eur. J. Inorg. Chem. 2003 (2003) 1058–1071.
[47] J.K. Norskov, T. Bligaard, A. Logadottir, J.R. Kitchin, J.G. Chen, S. Pandelov, U. Stimming, Trends in the exchange current for hydrogen evolution, J. Electrochem. Soc. 152 (2005) J23–J26.

Dr. Zegao Wang obtained his Ph.D. in Microelectronics and Solid-State Electronics from University of Electronic Science and Technology of China in 2014. Since 2014, he is a postdoctoral fellow in the Bio-SPM group, Aarhus University. His current research interest focuses on two-dimensional nanomaterials and their applications in electronic devices, biosensors and energy devices.

Dr. Qiang Li received his Ph.D. degree in Nanoscience in 2014 from Aarhus University, Denmark. He then worked as a postdoctoral fellow in the Bio-SPM group, Aarhus University. He is currently a professor in the School of Chemistry and Chemical Engineering at Shandong University since 2016. His research mainly focuses on the development of novel atomic force microscope technique for probing the physical and chemical properties at the nanoscale.

Haoxiang Xu received the B.S. degree (2014) in chemical engineering and technology at Beijing University of Chemical Technology, Beijing, China. He is currently a PhD candidate in Prof. Daojian, Cheng's lab. His research focuses on exploring mechanism of catalytic progress by multi-scale modeling, and high throughput theoretical design transition alloy nanocatalysts for clean energy conversion reactions.

Dr. Christian Dahl-Petersen obtained his M.Sc. in Engineering degree from the Technical University of Denmark (DTU) in Physics and Nanosystems in 2013. He received his Ph.D. degree from Aarhus University (AU) in 2016 for his research within surface catalysis in collaboration with Haldor Topsoe A/S. Currently, he is working within R&D in the sensor technology industry.

Qian Yang received her Bachelor degree (2013) in School of Chemistry and Chemical Engineering at Chongqing University, China. She is now a Ph.D candidate in School of Chemistry and Chemical engineering at Chongqing University. Her main research interests focus on the synthesis of 2D materials and design of heterogeneous catalytic material for photocatalysis and electrocatalysis application.

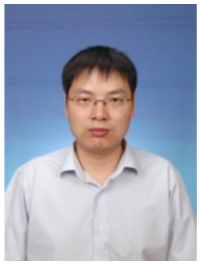

Dr. Daojian Cheng is currently a professor at Department of Chemical Engineering, Beijing University of Chemical Technology, China. Currently he has interests in theoretical study, computational design and experimental synthesis of metal clusters and nanoalloys as catalysts for renewable clean energy and environmental protection applications.

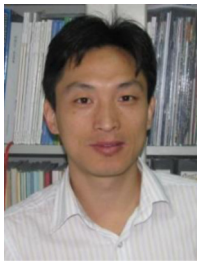

Dr. Dapeng Cao is a Fellow of the Royal Society of Chemistry (FRSC), and a Professor and Director of the Division of Molecular and Materials Simulation, State Key Laboratory of Organic-Inorganic Composites at Beijing University of Chemical Technology (BUCT) (2005-). He received his Ph.D. from BUCT in 2002, and was a research scientist at NanoMaterials Technology Pte Ltd in Singapore (2002–2003) and a postdoctoral researcher at the University of California at Riverside (2003–2005). His research interests are focused on the designed synthesis and applications of functional materials, including porous materials and energy materials related to fuel cells and supercapacitors.

Dr. Flemming Besenbacher received his doctoral degree in Natural Sciences from the Aarhus University (AU), Denmark. Since 1996 he is a professor at the Department of Physics of AU. His current research interests cover nanoscience, nanotechnology, nanocatalysis, scanning tunneling microscopy, atomic force microscopy, nucleation and growth of nanoclusters, interaction of hydrogen with defects in metals, hydrogen storage, and photocatalytic nanomaterials and biosensors.

Dr. Jeppe V. Lauritsen is associate professor at the Interdisciplinary Nanoscience Center at Aarhus University, Denmark. At iNANO, Dr. Jeppe V. Lauritsen leads a surface science group focusing on atomic-scale characterization of nanomaterials for energy applications incl. various metal sulfide, oxide or carbide compounds for use in both thermal and electrocatalysis.

Dr. Stig Helveg is Fellow at Haldor Topsoe A/S. He received the PhD degree in physics from the University of Aarhus, Denmark, in 2000 and then joined Haldor Topsoe A/S. He leads the company's efforts in in situ electron microscopy in catalysis. His current research focusses on the application and development of transmission electron microscopy for in situ studies of the structure, dynamics and function of heterogeneous catalysts at the atomic-scale.

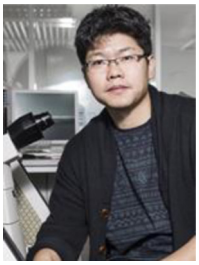

Dr. Mingdong Dong obtained his Ph.D. in Applied Physics from Aarhus University, Denmark in 2006. After postdoctoral research in Harvard University, he started his independent academic career as Assistant Professor and Associate Professor in Interdisciplinary Nanoscience Center (iNANO), Aarhus University. Currently, he is the group leader of Bio-SPM group. His research focuses on both the implementation and further development of a novel scanning probe microscope technique for studying new functional materials.